PROCEEDINGS OF SCIENCE

Dipole strength in N=50 nuclei studied in photon-scattering experiments at ELBE

R. Schwengner*[a], G. Rusev[a], N. Benouaret[a,b], R. Beyer[a], F. Dönau[a], M. Erhard[a], E. Grosse[a,c], A. R. Junghans[a], J. Klug[a], K. Kosev[a], C. Nair[a], N. Nankov[a,d], K. D. Schilling[a] and A. Wagner[a]

[a] *Institut für Strahlenphysik, Forschungszentrum Dresden-Rossendorf, 01314 Dresden, Germany*
[b] *Faculté de Physique, Université des Sciences et de la Technologie d'Alger, 16111 Bab-Ezzouar-Alger, Algerie*
[c] *Institut für Kern- und Teilchenphysik, Technische Universität Dresden, 01062 Dresden, Germany*
[d] *Institute for Nuclear Research and Nuclear Energy, BAS, 1784 Sofia, Bulgaria*
E-mail: r.schwengner@fzd.de

Dipole-strength functions up to the neutron-separation energies of the N=50 isotones ^{88}Sr, ^{89}Y and ^{90}Zr have been investigated in photon-scattering experiments using the bremsstrahlung facility at the superconducting electron accelerator ELBE of the Forschungszentrum Dresden-Rossendorf. A measurement using polarised bremsstrahlung impinging on ^{88}Sr revealed that the 50 most intense resolved transitions with energies greater than 6 MeV in this nuclide except for one are $E1$ transitions. These $E1$ transitions comprise about 63% of the total dipole strength of all ground-state transitions in ^{88}Sr. The intensity distributions obtained from the measured spectra after a correction for detector response and a subtraction of atomic background in the target contain a continuum part in addition to the resolved peaks. It turns out that the dipole strength in the resolved peaks amounts to about 40% of the total dipole strength while the continuum contains about 60%. In order to estimate the distribution of inelastic transitions and to correct the ground-state transitions for their branching ratios we performed simulations of γ-ray cascades. The photoabsorption cross sections obtained in this way connect smoothly to (γ,n) cross sections and give novel information about the strength on the low-energy tails of the Giant Dipole Resonances below the neutron-separation energies. In all three isotones extra dipole strength with respect to a parametrisation of the tail of the Giant Dipole Resonance with a Lorentz curve was observed in the energy range from about 6 to about 12 MeV. This extra strength may be an indication of a Pygmy Dipole Resonance in these nuclei. The experimental absorption cross sections are compared with predictions of a Quasiparticle-Random-Phase Approximation in a Woods-Saxon basis. The calculations also predict extra strength.

Workshop on Photon Strength Functions and Related Topics
June 17-20, 2007
Prague, Czech Republic

*Speaker.

PoS(PSF07)020

1. Introduction

The detailed understanding of the response of atomic nuclei to photons has received increasing attention in recent years. Information on the dipole strength at the low-energy tail of the Giant Dipole Resonance (GDR) is important for an estimate of the effect of high temperatures during the formation of heavy elements in the cosmos. In particular, reaction rates in the so-called p-process are influenced by the behaviour of dipole-strength functions close to the neutron-separation energy [1]. This behaviour may be affected by excitations like the Pygmy Dipole Resonance (see, e.g., Refs. [2, 3, 4]).

So far, estimates of the dipole strength obtained from calculations within a Quasiparticle-Random-Phase Approximation for spherical nuclei with a phenomenological implementation of nuclear deformation have been used for astrophysical applications [5, 6]. A systematic investigation of the dipole strength with varying nucleon numbers and, thus, varying properties like deformation is mandatory for the improvement of models that are used for modelling processes for the production of heavy elements in the cosmos. Dipole-strength functions up to the neutron-separation energies have been studied for only few nuclides in experiments with bremsstrahlung (see, e.g., Ref. [7] and Refs. therein). The new bremsstrahlung facility [8] at the superconducting electron accelerator ELBE of the research centre Dresden-Rossendorf opens up the possibility to study the dipole response of the stable nuclei with even the highest neutron-separation energies in photon-scattering experiments.

In order to obtain information on the influence of nuclear properties on the dipole response we have studied chains of nuclides with varying neutron or proton numbers, respectively. In the following, we describe especially the results of our experiments on the N=50 isotones ^{88}Sr, ^{89}Y and ^{90}Zr while results on the series of even-mass Mo isotopes from ^{92}Mo to ^{100}Mo are presented in the contribution by G. Rusev to these proceedings.

2. Experimental Methods

The nuclides ^{88}Sr, ^{89}Y and ^{90}Zr were studied in photon-scattering experiments at the superconducting electron accelerator ELBE of the research centre Dresden-Rossendorf. Bremsstrahlung was produced with electron beams of 9.0, 13.2, and 16.0 MeV kinetic energy in the case of ^{88}Sr, 9.5 and 13.2 MeV in the case of ^{89}Y and 7.6, 9.2 and 12.8 MeV in the case of ^{90}Zr. The average currents were chosen between 300 μA and 600 μA. The electron beams hit radiators consisting of niobium foils of 2, 4 or 7 μm thickness. A 10 cm thick aluminium absorber was placed behind the radiator in order to reduce the low-energy part of the bremsstrahlung spectrum. The collimated photon beam impinged onto the photon-scattering target with a flux of several 10^8 MeV^{-1} s^{-1} in a spot of 38 mm diameter. The target had a diameter of about 20 mm in order to enable an irradiation with a constant flux density over the target area. The targets consisted of 2731.8 mg of $^{88}SrCO_3$ enriched to 99.9%, 3300 mg of ^{89}Y and 4054.2 mg of $^{90}ZrO_2$ enriched to 97.7%, respectively. The targets were combined with 339.5 mg of ^{11}B used for the determination of the photon flux. Scattered photons were measured with four high-purity germanium (HPGe) detectors of 100 % efficiency relative to a 3 in. $\times$ 3 in. NaI detector. All HPGe detectors were surrounded by escape-suppression shields made of bismuth germanate scintillation detectors. Two HPGe detectors were

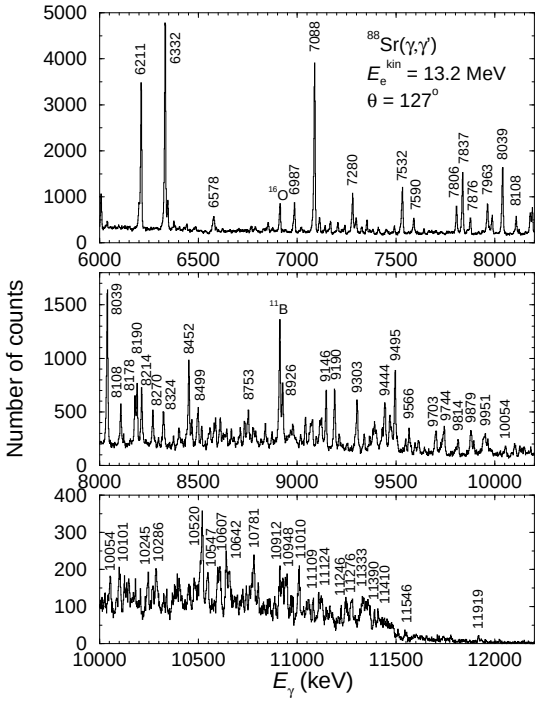

Figure 1: Parts of a spectrum of photons scattered from ^{88}Sr combined with ^{11}B during the irradiation with bremsstrahlung produced by electrons of an energy of $E_e^{\rm kin}$ = 13.2 MeV. This spectrum is the sum of the spectra measured with the two detectors placed at 127° relative to the beam. The most dominant transitions assigned to ^{88}Sr are marked with their energies in keV. The drop of intensity around 11.5 MeV is related to the opening of the (γ, n) channel.

placed vertically at 90° relative to the photon-beam direction at a distance of 28 cm from the target. The other two HPGe detectors were positioned in a horizontal plane and can be moved between 90° to the beam at a distance of 28 cm from the target and 127° to the beam at a distance of 32 cm from the target. The position at 90° allows us to measure azimuthal asymmetries of the γ-ray intensities in an experiment with polarised photons while the position at 127° allows us to deduce angular distributions of the γ rays. Absorbers of 3 mm Cu plus 3 or 8 mm Pb were placed in front of the detectors at 127° while for the detectors at 90° absorbers of 3mm Cu plus 8 or 13 mm Pb were used in the experiments at about 7, 9 or 13 MeV kinetic electron energy, respectively. A detailed description of the bremsstrahlung facility is given in Ref. [8].

Spectra of scattered photons were measured for 80 to 100 h in the various experiments. Parts of a spectrum including photons scattered from ^{88}Sr, measured with the two detectors placed at 127° relative to the beam at an electron energy of 13.2 MeV, are shown in Fig. 1.

2.1 Detector response and photon flux

For the analysis of the spectra the relative efficiency of the detectors and the relative photon flux are needed. Especially for the determination of the dipole-strength function described in Sec. 3 the experimental spectrum has to be corrected for detector response, for the absolute efficiency and the absolute photon flux, for background radiation, and for atomic processes induced by the

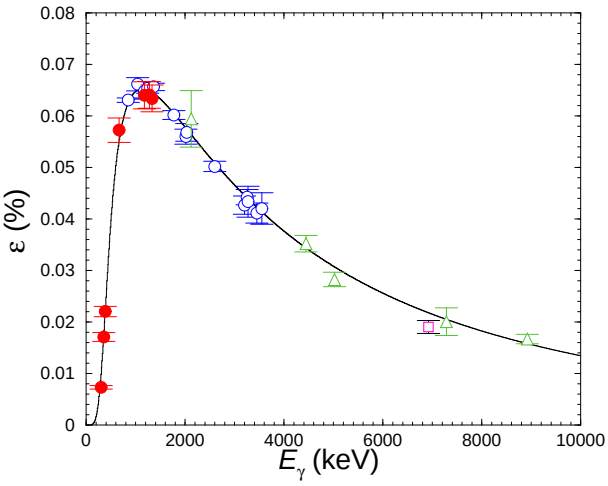

Figure 2: Absolute efficiency of the two detectors at 127° measured by using ^{22}Na, ^{60}Co, ^{133}Ba, and ^{137}Cs calibration sources (filled red circles) and simulated with the GEANT3 code (solid black line). In addition, relative efficiencies deduced from a ^{56}Co source (open blue circles), from transitions in ^{11}B (open green triangles) and ^{16}O (open magenta square) adjusted to the calculated curve as described in the text are given. The drop of efficiency below 1 MeV is due to absorbers in front of the detectors.

impinging photons in the target material. The detector response has been simulated by using the program package GEANT3 [9]. The absolute efficiency of the two HPGe detectors at 127° to the beam calculated by using GEANT3 is shown in Fig. 2. The absolute efficiency was determined experimentally up to 1332 keV from measurements of ^{22}Na, ^{60}Co, ^{133}Ba, and ^{137}Cs calibration sources. As shown in Fig. 2 experimental and simulated efficiencies agree well. An uncalibrated ^{56}Co source produced in-house using the ^{56}Fe$(p,n)^{56}$Co reaction was used to check the shape of the simulated efficiency curve up to 3.5 MeV. The relative efficiency values obtained from the ^{56}Co source were adjusted to the calculated value at 1238 keV and are consistent with the curve at higher energies (see Fig. 2).

The absolute photon flux was determined from intensities and the known integrated scattering cross section of transitions in ^{11}B which was combined with the respective target. For interpolation, the photon flux was calculated by using a code [10] based on the approximation given in Ref. [11] and including a screening correction according to Ref. [12]. This flux was corrected for absorption in the aluminium absorber placed behind the radiator and was then adjusted to the experimental values as is shown in Fig. 3. Several approaches to the calculation of the photon flux are discussed and compared with the flux derived from a measurement of protons emitted during the disintegration of deuterons in Ref. [8]. It was shown that the various approaches reproduce the experiment well. Therefore, we used the calculated flux to determine the relative efficiency of the detectors at the energies of transitions with known integrated scattering cross sections. This was done for a measurement with a $H_3^{11}BO_3$ target. From the intensities of transitions in ^{11}B and ^{16}O and the calculated photon flux we deduced values for the relative efficiency which were adjusted to the calculated value of the photon flux at 4444 keV and are shown in Fig. 2. The values are in good agreement with the calculated efficiency curve and prove its shape up to 9 MeV.

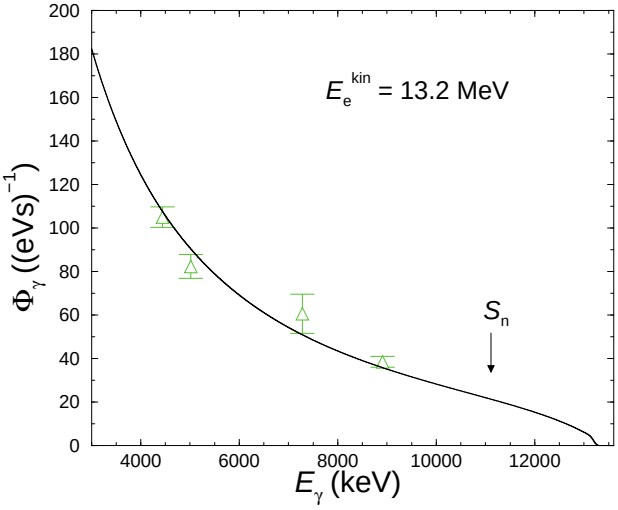

Figure 3: Absolute photon flux at the target deduced from intensities of transitions in ^{11}B (open green triangles) using the calculated efficiency shown in Fig. 2 and relative photon flux calculated as described in the text (solid black line).

2.2 Experiment with polarised photons

In order to determine the linear polarisation of γ transitions in ^{88}Sr we performed a photon-scattering experiment with polarised photons. Using two steering magnets the electron beam was deflected from the normal direction and then deflected back such that it hits the radiator in the center under a selected angle. As a consequence, an off-axis portion of the spatial distribution of the photons, which is partly polarised, is transmitted through the fixed collimator. The deflection angle for the production of polarised bremsstrahlung was chosen as $\theta = m_0c^2/E_e$, the ratio of the rest energy to the full energy of the electron, where a maximum degree of polarisation is expected [13]. The steering magnets were designed such that the electron beam can be deflected to four azimuthal angles of ϕ = 0°, 90°, 180°, and 270°, thus defining four different planes of polarisation. A cyclical use of these four directions enabled us to reduce the influence of fluctuations of the beam alignment and of uncertainties of e.g. the steerer adjustments.

The degree of polarisation was measured via the photodisintegration of the deuteron. Predominant $E1$ absorption above 4 MeV causes the emission of protons preferentially in the direction of the electric field vector of the polarised bremsstrahlung. The degree of polarisation can be deduced from azimuthal asymmetries of the intensities of the protons which were measured with four silicon detectors placed at polar angles of θ = 90° relative to the photon beam and at azimuthal angles of ϕ = 0°, 90°, 180°, and 270°, respectively. A polyethylene film of an areal density of 4 mg/cm^2, in which hydrogen is substituted by deuterium (CD2), was used as a target. The CD2 film was positioned parallel to the incident beam such that it was observed by all four detectors under 45°. Further details of the setup are given in Ref. [8].

The present experiment was carried out at a kinetic electron energy of 16 MeV with a measuring time of 200 h. The degree of polarisation P_γ was deduced from azimuthal asymmetries $P_\gamma\Sigma(\theta) = (\dot{N}_{p\parallel} - \dot{N}_{p\perp})/(\dot{N}_{p\parallel} + \dot{N}_{p\perp})$, where $\dot{N}_{p\parallel}$ and $\dot{N}_{p\perp}$ are the rates of protons resulting from

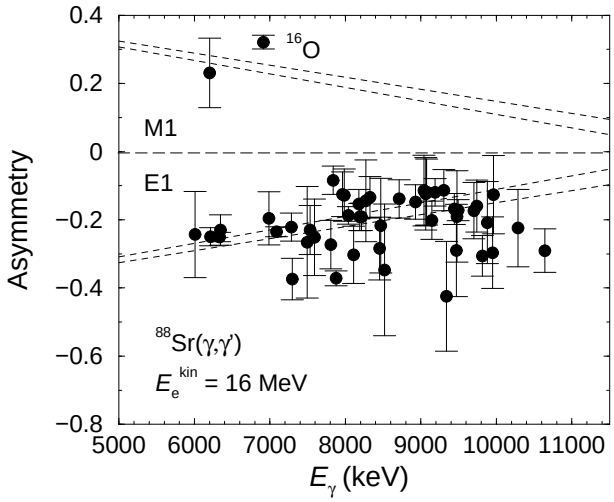

Figure 4: Experimental asymmetries $(\dot{N}_{\gamma\|} - \dot{N}_{\gamma\perp})/(\dot{N}_{\gamma\|} + \dot{N}_{\gamma\perp})$ of γ rays in ^{88}Sr. The bands marked with dashed lines indicate the degree of polarisation deduced from azimuthal asymmetries of the rates of protons emitted from disintegrating deuterons (see text). The data point marked ^{16}O belongs to a known $E2$ transition arising from the oxygen in the $^{88}SrCO_3$ target.

the disintegration of deuterons and measured perpendicular or parallel to the polarisation plane, respectively, and $\Sigma(\theta) = [W(\theta,\phi = 0^\circ) - W(\theta,\phi = 90^\circ)] / [W(\theta,\phi = 0^\circ) + W(\theta,\phi = 90^\circ)]$ is the analyzing power which is close to unity at an emission angle of $\theta = 90^\circ$ and the chosen geometry. Spectra measured with those detectors, which belong to the same orientation relative to the polarisation plane, were added up. The energies of the protons were rescaled to the energies of the incident photons according to $E_\gamma = E_p + E_n + E_\mathrm{B}$, where E_γ is the energy of the incident photon, $E_p \approx E_n$ are the kinetic energies of the proton and neutron, respectively, and E_B = 2225 keV is the binding energy of the deuteron.

Asymmetry values deduced for transitions in ^{88}Sr as $(\dot{N}_{\gamma\|} - \dot{N}_{\gamma\perp})/(\dot{N}_{\gamma\|} + \dot{N}_{\gamma\perp})$, where $\dot{N}_{\gamma\|}$ and $\dot{N}_{\gamma\perp}$ are the rates of γ transitions observed parallel or perpendicular to the polarisation plane, respectively, are depicted in Fig. 4. The values deduced for the transitions at 6212, 6333, 7088, 7837, and 8040 keV are consistent with those given in previous work [14]. The degree of polarisation derived as described above is also shown. Except for the transition at 6201 keV, all transitions above 6 MeV are $E1$ transitions. The transitions, which have been proven as $E1$ transitions, include 63% of the total dipole strength found for all transitions in the range from 6 to 12 MeV.

3. Determination of the dipole-strength function

In order to deduce the correct dipole-strength function, inelastic transitions have to be sorted out and the ground-state transitions have to be corrected for their branching ratios b_0. Since a definite and complete assignment of branching transitions to particular levels is not possible on the basis of the present experiment, we will use statistical methods to estimate the contributions of branching transitions and of the branching ratios of the ground-state transitions.

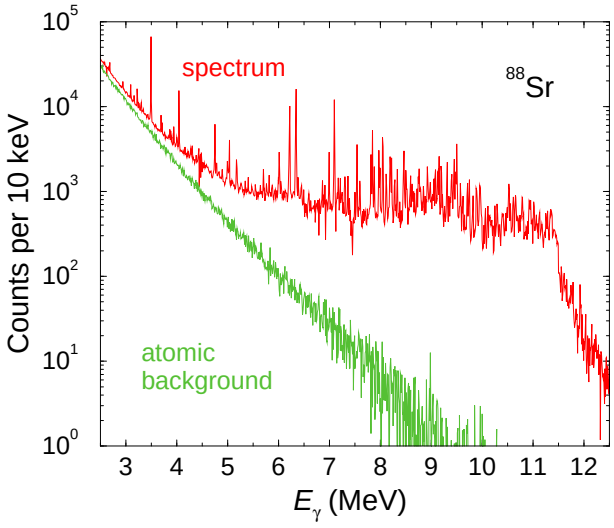

Figure 5: Experimental spectrum of ^{88}Sr (corrected for room background and detector response) and simulated spectrum of atomic background (multiplied with efficiency and measuring time).

In a first step spectra of the ambient background adjusted to the intensities of the 1460.5 keV transition (decay of ^{40}K) and 2614.9 keV transition (decay of ^{208}Tl) in the in-beam spectrum were subtracted from the measured spectra. It turned out that transitions following (n,γ) reactions in the HPGe detectors and in surrounding materials are negligibly small and thus, did not require correction. In order to correct the spectra for detector response, spectra of monoenergetic γ rays were calculated in steps of 10 keV by using GEANT3. Starting from the high-energy end of the experimental spectrum, the simulated spectra were subtracted sequentially. The resulting spectrum including the two detectors at 127° for the case of ^{88}Sr is shown in Fig. 5.

The background produced by atomic processes in the targets was obtained from a GEANT3 simulation using the absolute photon flux deduced from the intensities of the transitions in ^{11}B (cf. Fig. 3). The corresponding background spectrum for the ^{88}Sr target, multiplied with the efficiency curve shown in Fig. 2 and with the measuring time is also depicted in Fig. 5. As can be seen in Fig. 5 the continuum in the spectrum of scattered photons is clearly higher than the background by atomic scattering. This continuum may be formed by a large number of non-resolvable transitions with small intensities which are a consequence of the increasing nuclear level density at high energy and of Porter-Thomas fluctuations of the decay widths [15] in connection with the finite detector resolution (e.g. $\Delta E \approx 7$ keV at $E_\gamma \approx 9$ MeV).

The relevant intensity of the resonantly scattered photons is obtained from a subtraction of the atomic background from the response-corrected experimental spectrum. The remaining intensity distribution includes the intensity contained in the resolved peaks as well as the intensity of the "nuclear" continuum. The scattering cross sections $\sigma_{\gamma\gamma'}$ derived for energy bins of 0.2 MeV from the full intensity distribution are shown in Fig. 6. These values are compared with those for resolved transitions in ^{88}Sr. One sees that the two curves have similar structures caused by the prominent peaks. However, the curve including also the continuum part of the spectrum contains altogether a strength that is by a factor of about 2.3 greater than the strength of the resolved peaks only. In order

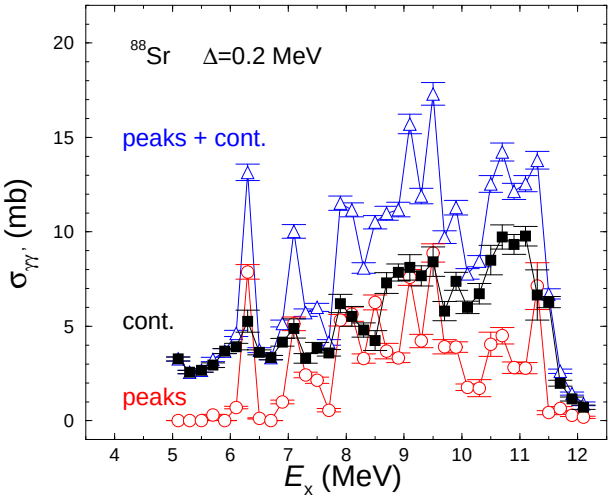

Figure 6: Scattering cross sections in ^{88}Sr, derived as $\sigma_{\gamma\gamma'} = \sum_{\Delta} I_s/\Delta$, not corrected for branching and averaged over energy bins of Δ = 0.2 MeV, as derived from the difference of the experimental spectrum and the atomic background shown in Fig. 5 ("peaks + cont.", open blue triangles) and from the resolved peaks only ("peaks", open red circles). In addition, the results of subtracting the values of the peaks from the spectrum that represent the continuum contribution, are shown ("cont.", black filled boxes) are shown.

to illustrate the contribution of the continuum, the difference of the two curves is also shown. In this curve representing the continuum only, the peak structures are washed out, thus proving that these structures are caused by the resolved peaks. The full intensity distribution (resolved peaks and continuum) and the corresponding scattering cross sections shown in Fig. 6 contain ground-state transitions and, in addition, branching transitions to lower-lying excited states (inelastic transitions) as well as transitions from those states to the ground state (cascade transitions). The different types of transitions cannot be clearly distinguished. However, for the determination of the photoabsorption cross section and the partial widths Γ_0 the intensities of the ground-state transitions are needed. Therefore, contributions of inelastic and cascade transitions have to be subtracted from the spectra. We corrected the intensity distributions by simulating γ-ray cascades [16] from the levels in the whole energy range analogously to the strategy of the Monte-Carlo code DICEBOX [17]. In these simulations, 1000 level schemes (nuclear realisations) starting from the ground state were created with level densities derived from the experiment [18]. We apply the statistical methods also for the low-energy part of the level scheme instead of using experimentally known low-lying levels in ^{88}Sr because this would require the knowledge of the partial decay widths of all transitions populating these fixed levels. Fluctuations of the nearest-neighbour-spacings were taken into account according to the Wigner distribution (see, e.g., Ref. [19]). The partial widths of the transitions to low-lying levels were assigned using a priori known strength functions for $E1$, $M1$, and $E2$ transitions. Fluctuations of the partial widths were treated by applying the Porter-Thomas distribution [15].

In the calculations, the recently published parameters for the Back-Shifted Fermi-Gas Model obtained from fits to experimental level densities [18] were used. In the individual nuclear realisations, the values of the parameters a and E_1 were varied within their uncertainties. We assumed

equal level densities for states with positive and negative parities at the same spin. This assumption has been recently justified by an investigation of level densities in the energy range from 5 to 10 MeV by using the ^{90}Zr(^{3}He,t) reaction [20].

For the $E1$, $M1$, and $E2$ photon strength functions Lorentzian parametrisations [21] were used. The parameters of the Lorentzian for the $E1$ strength were determined from a fit to (γ,n) data [22, 23, 24] in the energy range from 13 to 18 MeV. The obtained parameters σ_0 and Γ are consistent with the Thomas-Reiche-Kuhn sum rule [25] resulting in $\frac{\pi}{2}\sigma_0\Gamma = 60NZ/A$ MeV mb. The parameters for the $M1$ and $E2$ strengths were taken from global parametrisations of $M1$ spin-flip resonances and $E2$ isoscalar resonances, respectively [26].

Spectra of γ-ray cascades were generated for groups of levels in 100 keV bins in each of the 1000 nuclear realisations. For illustration, a mean intensity distribution of 1000 nuclear realisations including transitions depopulating levels in a 100 keV bin around 11 MeV is shown for the case of ^{88}Sr in Fig. 7 together with the distributions resulting from 10 individual nuclear realisations, which reflect the influence of fluctuations of level energies and level widths. Since in the nuclear realisations the levels were created randomly starting from the ground state instead of starting with the known first excited state at 1.8 MeV, the distribution of the branching transitions continues to the energy bin of the ground-state transitions. These spectra resemble qualitatively the ones measured in an experiment on ^{90}Zr using tagged photons [27]. Starting from the high-energy end of the experimental spectrum, which contains ground-state transitions only, the simulated intensities of the ground-state transitions were normalised to the experimental ones in the considered bin and the intensity distribution of the branching transitions was subtracted from the experimental spectrum. Applying this procedure step-by-step for each energy bin moving towards the low-energy end of the spectrum one obtains the intensity distribution of the ground-state transitions. Simultaneously, the branching ratios b_0^Δ of the ground-state transitions are deduced for each energy bin Δ. In an individual nuclear realisation, the branching ratio b_0^Δ is calculated as the ratio of the sum of the intensities of the ground-state transitions from all levels i to the total intensity of all transitions depopulating all levels i in Δ to any low-lying levels including the ground state. From dividing the summed intensities in a bin of the experimental intensity distribution of the ground-state transitions by the corresponding branching ratio we obtain the absorption cross section for a bin as $\sigma_\gamma^\Delta = \sigma_{\gamma\gamma}^\Delta / b_0^\Delta$. Finally, the absorption cross sections of each bin were obtained by averaging over the values of the 1000 nuclear realisations. For the uncertainty of the absorption cross section a 1σ deviation from the mean has been taken. The mean distribution of the calculated branching ratios b_0^Δ of 1000 nuclear realisations for the case of ^{88}Sr is shown in Fig. 7 together with the individual values of 10 nuclear realisations. The mean branching ratio decreases from about 80% for low-lying states, where only few possibilities for transitions to lower-lying states exist, to about 65% at the neutron-separation energy. Towards low energy the uncertainty of b_0^Δ increases due to level-spacing fluctuations and the decreasing level density. The large fluctuations below about 6 MeV make these values useless.

4. Results

The photoabsorption cross sections deduced from the present experiments for ^{88}Sr are shown in Fig. 8. Data of a previous experiment with monoenergetic photons in the energy range from

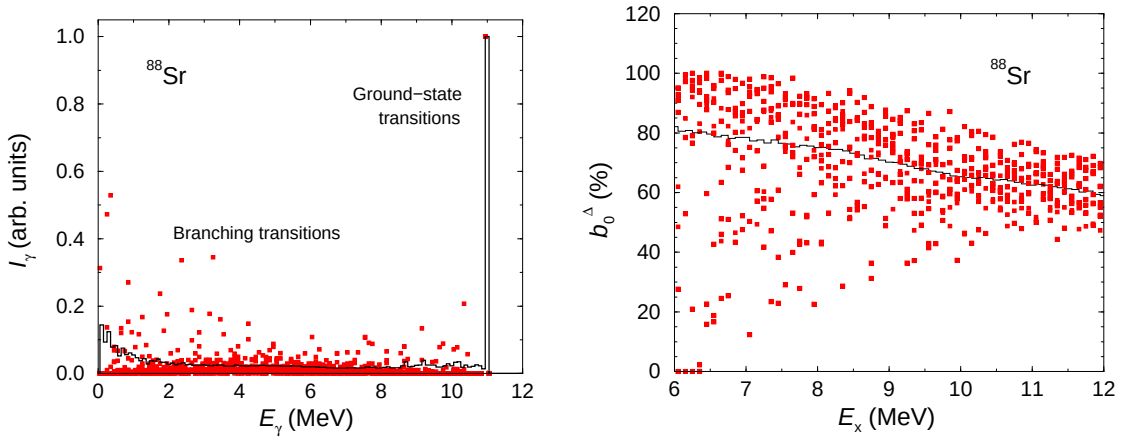

Figure 7: Left panel: Simulated intensity distribution of transitions depopulating levels in a 100 keV bin around 11 MeV in ^{88}Sr. The black line represents the mean distribution of 1000 nuclear realisations. The red squares depict the intensities obtained in 10 individual nuclear realisations. Right panel: Branching ratios of ground-state transitions as obtained from the simulations of γ-ray cascades for ^{88}Sr. The black line represents the mean distribution of 1000 nuclear realisations. The red squares represent the values of 10 individual nuclear realisations.

8.6 to 12 MeV [28] are also shown. The present photon-scattering data are compared with the data of (γ,n) experiments [22, 23]. The cross sections of the (γ,p) reaction are very small in the considered energy range and were therefore neglected.

The photoabsorption cross sections obtained from the present (γ,γ') experiments after the described correction are consistent with the cross sections obtained from the experiment with monoenergetic photons. The comparison of the present data with (γ,n) data shows a smooth connection between the data of the two different experiments. Consequently, the present (γ,γ') data provide new information about the continuation of the dipole-strength function below the threshold of the (γ,n) reaction.

The total photoabsorption cross sections have been deduced by combining the present (γ,γ') data, the (γ,p) data and the (γ,n) data. These total absorption cross sections for ^{88}Sr, ^{89}Y and ^{90}Zr are shown in Figs. 9, 10 and 11, respectively. Note that the data obtained from the present photon-scattering experiments for ^{89}Y and ^{90}Zr are preliminary. These data were combined with the respective (γ,n) data for ^{89}Y [22] and for ^{90}Zr [24]. The cross sections of the (γ,p) reactions have been taken from Ref. [29] for the two nuclides. The experimental total cross sections are compared with Lorentz curves (E_0 = 16.8 MeV, Γ = 4.0 MeV) fulfilling the Thomas-Reiche-Kuhn sum rule. As can be seen in Figs. 9, 10 and 11 the experimental cross sections include extra strength with respect to the approximation of the GDR by a Lorentz curve in the energy range from about 6 to about 11 MeV. According to the measurement with polarised photons described in Sec. 2.2 we can assume $E1$ character for this extra strength which amounts to about 2% of the Thomas-Reiche-Kuhn sum rule and may be related to a Pygmy Dipole Resonance. In order to compare the experimental findings with theoretical predictions we have performed calculations within the framework of the quasiparticle-random-phase approximation (QRPA).

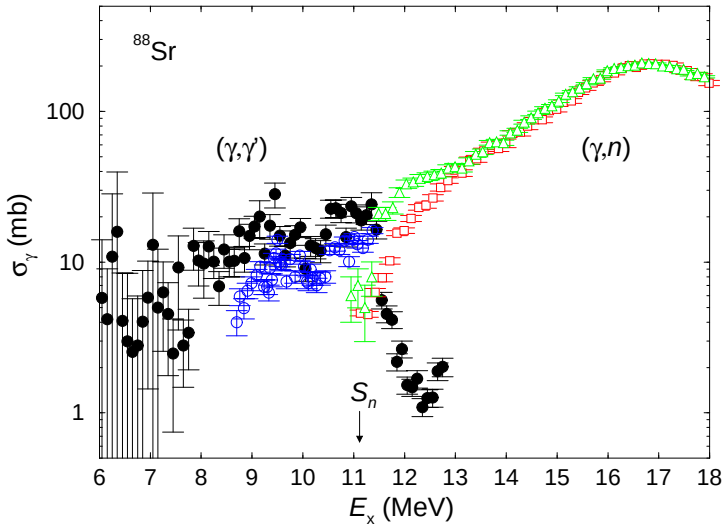

Figure 8: Photoabsorption cross sections deduced from the present photon-scattering data for ^{88}Sr according to $\sigma_\gamma = \sigma_{\gamma\gamma}/b_0$ after correction for branching transitions (filled black circles) in comparison with data obtained from an experiment with monoenergetic photons (open blue circles) [28] and with photoabsorpton cross sections obtained from (γ,n) experiments taken from Ref. [22] (open green triangles) and Ref. [23] (open red squares).

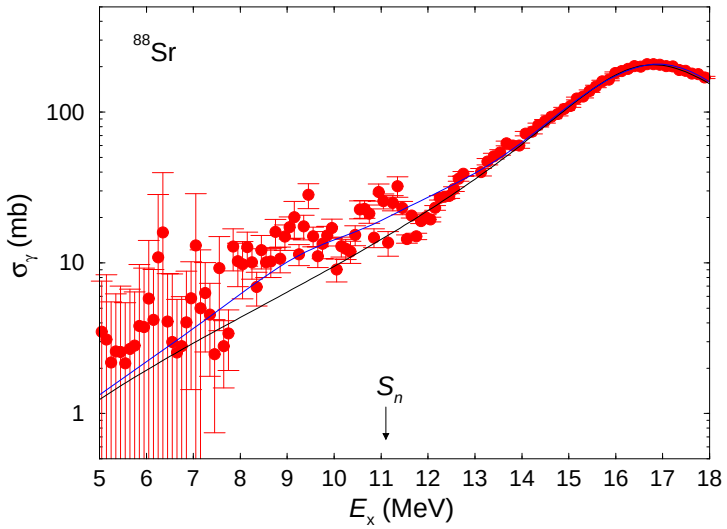

Figure 9: Total photoabsorption cross section for ^{88}Sr obtained by combining the present (γ,γ') data and the (γ,n) data of Refs. [22, 23] (red circles). For the (γ,n) data mean values of the data given in Refs. [22, 23] have been used as those data disagree in the range between 11 and 13 MeV (cf. Fig. 8). The black line shows a Lorentz distribution with parameters given in the text. The blue line is the result of QRPA calculations, where the discrete values were folded with a Lorentzian of a width Γ = 3.2 MeV.

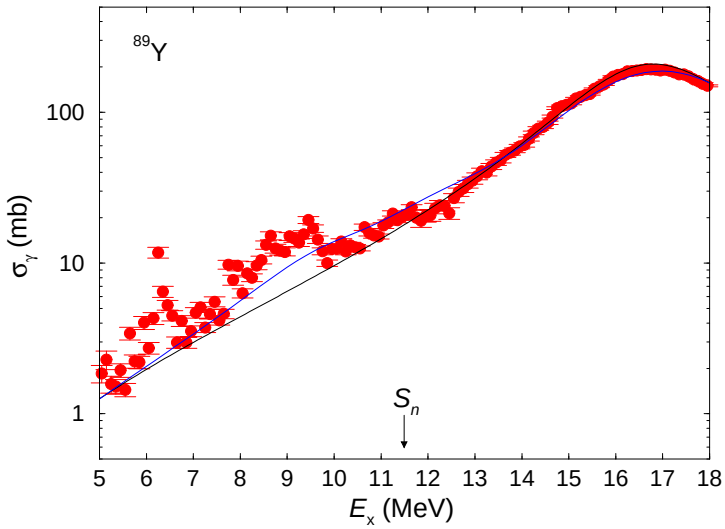

Figure 10: Total photoabsorption cross section for ^{89}Y obtained by combining the present (γ,γ') data, the (γ,n) data of Ref. [22] and the (γ,p) data of Ref. [29] (red circles). The black line shows a Lorentz distribution with parameters given in the text. The blue line is the result of QRPA calculations, where the discrete values were folded with a Lorentzian of a width Γ = 3.2 MeV.

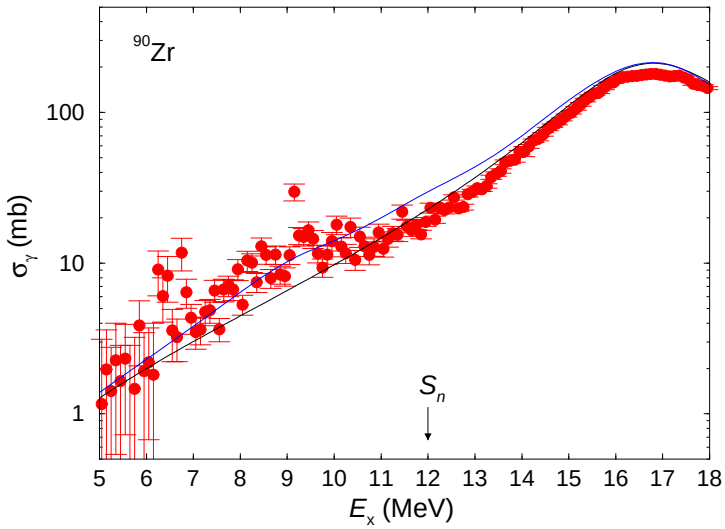

Figure 11: Total photoabsorption cross section for ^{90}Zr obtained by combining the present (γ,γ') data, the (γ,n) data of Ref. [24] and the (γ,p) data of Ref. [29] (red circles). The black line shows a Lorentz distribution with parameters given in the text. The blue line is the result of QRPA calculations, where the discrete values were folded with a Lorentzian of a width Γ = 3.2 MeV.

5. QRPA calculations

The QRPA calculations used a Woods-Saxon basis, a separable dipole-plus-octupole interaction and the nuclear selfconsistency approach [30]. The possible contamination of the calculated $E1$ strength with spurious motion of the centre-of-mass is completely removed by means of the suppression method described in Ref. [31]. The relative strength of the isovector part of the dipole-plus-octupole interaction was adjusted such that it reproduces the position of the maximum of the GDR. The model is described in detail in Ref. [32]. Similar QRPA calculations were also performed in our recent study of the magnetic-dipole $(M1)$ strength in Mo isotopes [33].

The photoabsorption cross sections calculated for ^{88}Sr, ^{89}Y and ^{90}Zr are compared with the experimental data in Figs. 9, 10 and 11, respectively. As can be seen the calculations also predict extra strength in addition to the approximation of the GDR by a Lorentz curve but underestimate the experimental extra strength.

6. Summary

We have studied of dipole-strength functions of the N = 50 isotones ^{88}Sr, ^{89}Y and ^{90}Zr up to the neutron-separation energies at the photon-scattering facility of the electron accelerator ELBE. A measurement of linear polarisations of the γ rays in ^{88}Sr by using polarised bremsstrahlung reveals that almost all transitions with energies greater than 6 MeV are $E1$ transitions which comprise about 63% of the total dipole strength of all ground-state transitions. A comparison of a measured spectrum with the calculated atomic background shows that about 40% of the total dipole strength is located in resolved peaks and about 60% in a continuum part of the spectrum. In order to estimate intensities of branching transitions we performed simulations of statistical γ-ray cascades. The absorption cross sections obtained after subtraction of intensities of branching transitions from the experimental intensity distributions and correction of the intensities of the ground-state transitions for their branching ratios connect smoothly with (γ,n) data. We observed extra strength with respect to a Lorentz parametrisation of the GDR in the energy range from 6 to 11 MeV. QRPA calculations predict also extra strength in this energy range but underestimate the experimental extra strength.

This work was supported by the Deutsche Forschungsgemeinschaft under contract DO466/1-2.

References

[1] M. Arnould and S. Goriely, Phys. Rep. **384**, 1 (2003).

[2] G. A. Bartholomew, E. D. Earle, A. J. Ferguson, J. W. Knowles, and M. A. Lone, Adv. Nucl. Phys. **7**, 229 (1972).

[3] S. Goriely, Phys. Lett. B **436**, 10 (1998).

[4] A. Zilges, M. Babilon, T. Hartmann, D. Savran, and S. Volz, Progr. Part. Nucl. Phys. **55**, 408 (2005).

[5] S. Goriely and E. Khan, Nucl. Phys. A **706**, 217 (2002).

[6] S. Goriely, E. Khan, and M. Samyn, Nucl. Phys. A **739**, 331 (2004).

[7] U. Kneissl, N. Pietralla, and A. Zilges, J. Phys. G: Nucl. Part. Phys. **32**, R217 (2006).

[8] R. Schwengner, R. Beyer, F. Dönau, E. Grosse, A. Hartmann, A. R. Junghans, S. Mallion, G. Rusev, K. D. Schilling, W. Schulze, and A. Wagner, Nucl. Instr. Meth. A **555**, 211 (2005).

[9] CERN Program Library Long Writeup W5013, Geneva 1993, unpublished.

[10] E. Haug, private communication.

[11] G. Roche, C. Ducos, and J. Proriol, Phys. Rev. A **5**, 2403 (1972).

[12] F. Salvat, J.D. Martinez, R. Mayol, and J. Parellada, Phys. Rev. A **36**, 467 (1987).

[13] M. May and G. C. Wick, Phys. Rev. **81**, 628 (1951).

[14] K. Wienhard, C. Bläsing, K. Ackermann, K. Bangert, U. E. P. Berg, K. Kobras, W. Naatz, D. Rück, R. K. M. Schneider, and R. Stock, Z. Phys. A **302**, 185 (1981).

[15] C. E. Porter and R. G. Thomas, Phys. Rev. **104**, 483 (1956).

[16] G. Rusev, Dissertation, Technische Universität Dresden, 2007, unpublished.

[17] F. Bečvář, Nucl. Instr. Meth. A **417**, 434 (1998).

[18] T. von Egidy and D. Bucurescu, Phys. Rev. C **72**, 044311 (2005).

[19] T. A. Brody, J. Flores, J. B. French, P. A. Mello, A. Pandey, and S. S. M. Wong, Rev. Mod. Phys. **53**, 385 (1981).

[20] Y. Kalmykov, T. Adachi, G. P. A. Berg, H. Fujita, K. Fujita, Y. Fujita, K. Hatanaka, J. Kamiya, K. Nakanishi, P. von Neumann-Cosel, V. Yu. Ponomarev, A. Richter, N. Sakamoto, Y. Sakemi, A. Shevchenko, Y. Shimbara, Y. Shimizu, F. D. Smit, T. Wakasa, J. Wambach, and M. Yosoi, Phys. Rev. Lett. **96**, 012502 (2006).

[21] P. Axel, Phys. Rev. **126**, 671 (1962).

[22] A. Lepretre, H. Beil, R. Bergere, P. Carlos, A. Veyssiere, and M. Sugawara, Nucl. Phys. **A175**, 609 (1971).

[23] A. M. Goryachev and G. N. Zalesnyy, Vopr. Teor. Yad. Fiz. **8**, 121 (1982).

[24] B. L. Berman, J. T. Caldwell, R. R. Harvey, M. A. Kelly, R. L. Bramblett, and S. C. Fultz, Phys. Rev. **162**, 1098 (1967).

[25] P. Ring and P. Schuck, in *The Nuclear Many Body Problem*, (Springer, New York, 1980).

[26] http://www-nds.iaea.org/RIPL-2/.

[27] R. Alarcon, R. M. Laszewski, A. M. Nathan, and S. D. Hoblit, Phys. Rev. C **36**, 954 (1987).

[28] S. Datta and J. S. Allen, Phys. Rev. C **8**, 1421 (1973).

[29] T. Rauscher and F.-K. Thielemann, At. Data Nucl. Data Tables **88**, 1 (2004).

[30] H. Sakamoto and T. Kishimoto, Nucl. Phys. A **501**, 205 (1989).

[31] F. Dönau, Phys. Rev. Lett. **94**, 092503 (2005).

[32] F. Dönau, G. Rusev, R. Schwengner, A. R. Junghans, K. D. Schilling, and A. Wagner, Phys. Rev C **76**, 014317 (2007).

[33] G. Rusev, R. Schwengner, F. Dönau, M. Erhard, S. Frauendorf, E. Grosse, A.R. Junghans, L. Käubler, K. Kosev, L.K. Kostov, S. Mallion, K.D. Schilling, A. Wagner, H. von Garrel, U. Kneissl, C. Kohstall, M. Kreutz, H.H. Pitz, M. Scheck, F. Stedile, P. von Brentano, C. Fransen, J. Jolie, A. Linnemann, N. Pietralla, V. Werner, Phys. Rev. C **73**, 044308 (2006).